Available online at www.sciencedirect.com
SCIENCE DIRECT®
Pergamon
Acta Materialia 51 (2003) 4761–4772
Acta MATERIALIA
www.actamat-journals.com

Phase field study of grain boundary effects on spinodal decomposition

H. Ramanarayan, T.A. Abinandanan *

Department of Metallurgy, Indian Institute of Science, Bangalore 560 012, India

Received 10 February 2003; received in revised form 2 May 2003; accepted 28 May 2003

Abstract

We have developed a phase field model of a polycrystalline alloy by combining the Cahn–Hilliard model [J Chem Phys 28 (1958) 258] with a model of polycrystals due to Fan and Chen [Acta Mater 45 (1997) 3297]. We have used this model to study grain boundary (GB) effects on spinodal decomposition (SD) in two-dimensional (2D) systems. In binary A–B systems with constant atomic mobility, when the GB-energy (γ_α) of the A-rich α phase is lower than that (γ_β) of the B-rich β phase, decomposition starts by enriching the GB with species A, setting off a composition wave that produces alternating α and β bands near the GB. Simultaneously, the grain interiors undergo normal SD. Thus, when decomposition ends, GB-bands coexist with grain interiors with spinodal microstructure. The number of GB bands is rationalized in terms of ($\gamma_\beta - \gamma_\alpha$) and the rate of SD in the grain interior. Further, during decomposition, grain growth is effectively suppressed.

Keywords: Spinodal decomposition; Grain boundaries; Phase field models; Coarsening

1. Introduction

Phase separation, and spinodal decomposition (SD) in particular, have been studied extensively in *bulk* alloys using a variety of theoretical, computational and experimental techniques (see Refs. [3–6] for recent reviews). In recent years, however, the focus has been on the effect of various *defects* on these processes. For example, the effect of a free surface on SD has been studied using computer simulations [7–15], and experiments on polymeric blends [16].

Similarly, the effect of dislocations in a phase separating alloy (outside the spinodal) has been studied by Hu and Chen [17]. More recently, the effect of precipitate plates on SD in the inter-precipitate regions in an Al–Ag alloy has been studied experimentally by Moore et al. [18]. In this paper, we present the results from computer simulations of grain boundary (GB) effects on SD in two-dimensional (2D) systems.

Since GB's are planar defects, *some* of their effects may be similar to those of a free surface, investigated extensively [7–15]. However, GB's differ from free surfaces in important ways. Struc-

* Corresponding author. Tel.: +91-80-394-2676; fax: +91-80-360-0472.
E-mail address: abinand@metalrg.iisc.ernet.in (T.A. Abinandanan).

1359-6454/$30.00
doi:10.1016/S1359-6454(03)00301-X

turally, GB's are internal interfaces, while surfaces are the system's external boundary. Further, in a spinodally decomposing system with a surface, there are three possible boundaries: surfaces of the two product phases α and β, and the coherent α–β interface; in a polycrystalline system with GB's, however, four possible boundaries can be formed as a result of SD: α-GB, β-GB, coherent α–β interface and incoherent α–β interface. In other words, the equivalent of an incoherent α–β interface (i.e., the two phases across this boundary have different orientations) does not exist in studies of surface effects on SD. More importantly, GB's, unlike free surfaces, have the freedom to migrate in a direction normal to themselves [19]. Thus, GB effects on SD deserve to be studied in their own right; similarities and differences between GB and surface effects are discussed further in Section 4.

Computer simulations of SD in bulk systems use either atomistic models or continuum models (see the reviews [3–6], and references therein). In the latter case, simulations are based on solving the Cahn–Hilliard equation [20], which accounts adequately for the compositionally diffuse, coherent α–β interface. In modelling SD in *polycrystalline alloys*, however, three other types of boundaries (α-GB, β-GB and incoherent α–β boundaries) must also be accounted for. Our model achieves this purpose by combining the Cahn–Hilliard model with a phase field model for a polycrystal; the latter was employed by Fan and Chen [2] for studying grain growth in a pure component.

We have organized this paper as follows: after presenting the details of our computational model and the resulting kinetic equations in Section 2, we present in Section 3 the results from our study of 2D systems with constant, position-independent atomic mobility. In Section 4, we discuss our results and their implications. We summarize the key conclusions from this work in Section 5.

2. Model

We need a model for a *polycrystalline alloy* for studying GB effects on SD in a binary system. For this purpose, we use a combination of the classical Cahn–Hilliard formalism for a compositionally inhomogeneous alloy [1,20] and Fan and Chen's phase field model [2] for a polycrystal. The former is developed using the composition field $c(\mathbf{r})$ in an alloy. In a similar way, the model of Fan and Chen is developed using a set of n 'orientational' (and non-conserved) order parameter fields $\eta_i(\mathbf{r})$ (i = 1,2,...,n) to represent n different grain orientations in the microstructure; η_i are continuum analogues of Potts variables in the n-state Potts model [21,22]. Each η_i takes a finite equilibrium value (taken to be unity) within the ith grain and drops to zero outside it, through a GB region where it varies smoothly. Thus, an instantaneous configuration in our model is described in terms of the n + 1 position-dependent field variables (c; $\eta_1,\eta_2,...,\eta_n$). The local composition c used in our model is defined as follows:

$$c = \frac{c' - c'_\alpha}{c'_\beta - c'_\alpha}$$

where c' is the local composition, c'_α and c'_β are the equilibrium compositions of the A-rich α and B-rich β phases, respectively; all are expressed in mole fraction of species B. Thus, c = 0 and c = 1 correspond to α and β phases, respectively.

Cahn–Hilliard theory [1,20] for a conserved variable and Cahn–Allen theory [23] for non-conserved variables (the model of Fan and Chen belongs to this category) are well established in the literature [3–6]. Therefore, we present only an outline of our model in this section. Further, our model is presented using dimensionless quantities. We non-dimensionalize all the quantities using a characteristic energy E', length L' and time T'; our choices for them are presented at the end of the formulation in Section 2.3.

2.1. Energetics

In the spirit of diffuse interface models, the total free energy, F, of a system with inhomogeneities in both c and η_i is written as a volume integral:

$$F = N_V \int_V \left[f(c,\eta_i) + \kappa_c(\nabla c)^2 + \sum_i \kappa_i(\nabla \eta_i)^2 \right] \mathrm{d}V, \quad (1)$$

where N_V is the (constant) number of atoms per unit volume, $f(c,\eta_i)$ is the Helmholtz free energy per atom of a bulk homogeneous alloy and, κ_c and κ_i are the (constant) gradient energy coefficients associated with inhomogeneities in composition and in η_i, respectively. We further assume $\kappa_i = \kappa_\eta$ for all i.

At low temperatures, equilibrium in a phase separating alloy is characterized by co-existence of two phases: α and β. Further, the crystals of each of these phases could have any of the n possible grain orientations. Thus, the bulk free energy density $f(c,\eta_i)$ is chosen such that it exhibits a minimum for these $2n$ possibilities. In other words, f has $2n$ degenerate minima (whose value is chosen to be zero, for convenience) in the $(n+1)$-dimensional space spanned by $(c;\eta_1,\eta_2,...,\eta_n)$; these minima are located at n grains of α with a composition of $c = 0$:

(0;1,0,…,0), (0;0,1,…,0),…,(0;0,0,…,1),

and n grains of β with a composition of $c = 1$:

(1;1,0,…,0), (1;0,1,…,0),…,(1;0,0,…,1).

We use the following form for $f(c,\eta_i)$:

$$f(c,\eta_i) = f_o(c) + m(c)\left\{0.25 + \sum_i\left[-\frac{\eta_i^2}{2} + \frac{\eta_i^4}{4}\right] + \varepsilon\sum_{i}\sum_{j>i}\eta_i^2\eta_j^2\right\}, \quad (2)$$

where $f_o(c)$ is the free energy per atom in a bulk single crystal of composition c given by:

$$f_o(c) = A_c c^2(1-c)^2, \quad (3)$$

the constant A_c determines the height of the free energy barrier between the equilibrium phases within a single gran, $m(c)$ is a composition dependent factor which couples the composition with the orientational order parameters η_i and ε is a constant. The constant 0.25 within the curly braces in Eq. (2) is used as a convenient way to ensure that $f(c,\eta_i) = 0$ at each of the $2n$ degenerate minima.

For a single crystal in which $\{\eta_i\} = (1,0,0,...,0)$ everywhere, Eq. (1) reduces to: $F = N_V\int_V [f(c) + \kappa_c(\nabla c)^2]\,dV$, the starting point for the Cahn–Hilliard model [1]. Similarly, for an alloy of composition $c = 0$, say, Eq. (1) reduces to an equation similar to the one in the model of Fan and Chen [2]. The factor $m(c)$ glues the two models together; as shown in the next section, it plays an important role in determining the relative values of the GB energies of α and β phases, and of the energy of the incoherent interface between them.

We note briefly that, in Eq. (2), the terms within the curly braces are even functions of η_i; therefore, $f(c,\eta_i)$ has additional degenerate minima at $2n$ more locations with negative values of η_i such as $\{c;\eta_i\} = (0;-1,0,...,0),....$ In our computer simulations, these extra degenerate equilibrium states are excluded by working only with $\eta_i \geq 0$.

2.2. Kinetics

The evolution of the composition field c is governed by the Cahn–Hilliard equation for conserved variables [1,20]:

$$\frac{dc}{dt} = M\nabla^2\left[\frac{\delta(F/N_V)}{\delta c}\right], \quad (4)$$

where $\delta(F/N_V)/\delta c = \mu$ is the chemical potential whose gradient drives diffusion, and M is the atomic mobility. Similarly, the evolution of order parameter fields η_i is governed by the Cahn–Allen equation for non-conserved variables:

$$\frac{d\eta_i}{dt} = -L_i\left[\frac{\delta(F/N_V)}{\delta\eta_i}\right], \quad (5)$$

where $\delta(F/N_V)/\delta\eta_i$ are the variational derivatives of (F/N_V), the total free energy (per atom) with respect to η_i, and L_i are the relaxation coefficients for η_i. In this study, M and $L_i = L$ $(i = 1,2,...,n)$ are assumed to be constants.

2.3. Non-dimensionalization

The characteristic length L', energy E' and time T' used for rendering all the quantities dimensionless are chosen in such a way that each of the quantities A_c (in Eq. (3)), κ_c (in Eq. (1)) and M (in Eq. (4)) takes a value of unity. Thus, our choices are: $L' = (\kappa'_c/A'_c)^{(1/2)}$, $E' = A'_c L'^3$ and $T' = L'^2(c'_\beta - c'_\alpha)^2/(M'E')$, where A'_c, κ'_c and M' are

dimensional equivalents of A_c, κ_c and M, respectively. Nevertheless, our formulation has been presented in such a way that the equations are valid even when all the dimensionless quantities in them are replaced by their respective dimensional counterparts.

2.4. Numerical implementation

The numerical method used in our simulations is based on the semi-implicit Fourier spectral method developed by Zhu et al. [24]. Expanding the Cahn–Hilliard equation (Eq. (4)), we get:

$$\frac{\partial c}{\partial t} = M\nabla^2[g(c) - 2\kappa_c\nabla^4 c], \tag{6}$$

where $g(c) = \delta f/\delta c$. Fourier transformation of this equation yields:

$$\frac{\partial \tilde{c}(\mathbf{k},t)}{\partial t} = -M(k^2 g(\tilde{\mathbf{k}},t) + 2\kappa_c k^4 \tilde{c}(\mathbf{k},t)), \tag{7}$$

where $\tilde{c}(\mathbf{k},t)$ and $\tilde{g}(\mathbf{k},t)$ are Fourier transforms of $c(\mathrm{r},t)$ and $g(\mathrm{r},t)$, respectively. Using backward differencing for $\partial\tilde{c}/\partial t$, this equation can be rewritten as

$$\frac{\tilde{c}(\mathbf{k},\mathrm{t}+\Delta t) - \tilde{c}(\mathbf{k},\mathrm{t})}{\Delta t} = -M[k^2\tilde{g}(\mathbf{k},t+\Delta t) + 2\kappa_c k^4 \tilde{c}(\mathbf{k},\mathrm{t}+\Delta t)]. \tag{8}$$

Using the approximation $\tilde{g}(\mathbf{k},t+\Delta t) \approx \tilde{g}(\mathbf{k},t)$, the above equation may be rearranged to yield the following semi-implicit form:

$$\tilde{c}(\mathbf{k},t+\Delta t) = \frac{\tilde{c}(\mathbf{k},t) - \Delta t M k^2 \tilde{g}(\mathbf{k},t)}{1 + 2\Delta t M \kappa_c k^4}, \tag{9}$$

in which all the terms on the right hand side are evaluated at time t. A similar procedure for the Cahn–Allen equation (Eq. (5)) results in the following:

$$\tilde{\eta}_i(\mathbf{k},t+\Delta t) = \frac{\tilde{\eta}_i(\mathbf{k},t) - \Delta t L_i \tilde{h}_i(\mathbf{k},t)}{1 + 2\Delta t L_i \kappa_\eta k^2}, \tag{10}$$

where $\tilde{\eta}_i(\mathbf{k},t)$ and $\tilde{h}_i(\mathbf{k},t)$ are Fourier transforms of $\tilde{\eta}_i(\mathbf{r},t)$ and $h_i(\mathbf{r},t)$, respectively, and $h_i = \partial f/\partial\eta_i$.

3. Results

3.1. Boundary energies and widths

We have listed in Table 1 those model parameters which are the same in all our calculations. We have studied four different systems with different combinations of $m(c)$ and κ_i; we discuss below the rationale behind our choice of systems.

In our model, $m(c)$ in Eq. (2) couples c and η_i, and determines, through the product $\varepsilon m(c)$, the height of the free-energy barrier traversed by (η_i,η_j) as they go from (1,0) in the ith grain to (0,1) in the jth grain. Thus, it determines the composition dependence of GB energy (since ε is constant). In this paper, we focus our attention on two different systems, referred to as Ia and IIa: in system Ia, $m(c) = 1+0.5c^2$ and in system IIa, $m(c) = 1+0.1c^2$. These expressions for $m(c)$ translate into $(\gamma_\beta - \gamma_\alpha)/\gamma_\alpha$ values of 0.22 and 0.05 in systems Ia and IIa, respectively, where γ_β and γ_α are the GB energies of the β and α phases, respectively.

The figures in the left column in Fig. 1 show the equilibrium profiles of c, η_1 and η_2 normal to the four different planar boundaries in system Ia. These profiles were obtained by simulating to equilibrium a system containing each of these planar interfaces of unit area (i.e., by solving the Cahn–Hilliard and Cahn–Allen equations until the c and η_i fields become stationary along the direction nor-

Table 1
List of parameters used in this study

Model parameter	Value
A	1.0
κ_c	1.0
M	1.0
ε	2.0
$\kappa_i = \kappa_\eta$	1.0
$L_i = L$	1.0
Simulation parameter	**Value**
$\Delta x = \Delta y$	1.0
Δt	0.1
$N_x \times N_y$	512×256 (two-grain case)
	512×512 (polycrystalline case)

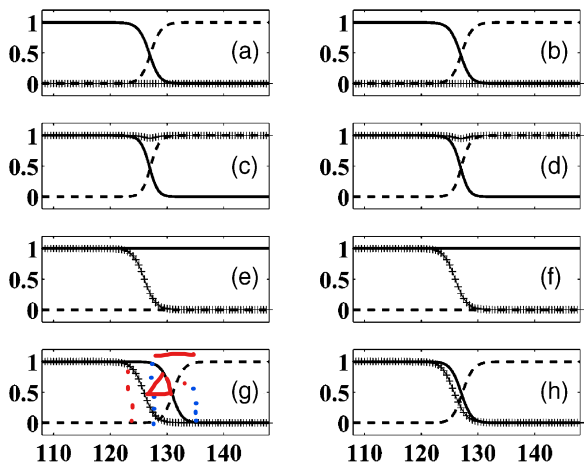

Fig. 1. Equilibrium profiles of c (drawn with the '+' symbol), η_1 (continuous line) and η_2 (dashed line) as a function of distance normal to the following planar interfaces: grain boundary in α(a, b) and β(c, d) phases, coherent interface (e, f) and incoherent interface (g, h). The left and right columns are for systems Ia and Ib, respectively.

mal to the interface). They are used for calculating the interfacial energies and widths, as described below. For α-GB and β-GB (Fig. 1a,c), composition is the same ($c = 0$ and $c = 1$, respectively) in the two grains, whose orientations are different: in the left and right grains, (η_1,η_2) values are (1,0) and (0,1), respectively. For the coherent α–β boundary (Fig. 1e), the composition changes from $c = 1$ to $c = 0$, while $(\eta_1,\eta_2) = (1,0)$ remain constant, indicating that the two phases have the same grain orientation (i.e., they are within the same grain). Finally, Fig. 1g for the incoherent boundary shows that the β grain on the left and the α grain on the right have different grain orientations.

Fig. 1g, for system Ia, also displays an interesting feature: the regions of sharp gradients in c and η_i are separated by a distance which is about half of the GB width; i.e., this boundary is essentially a combination of a coherent boundary and α-GB. Indeed, γ_i, the incoherent interface energy for this system in Table 2 is also nearly the same as the sum of γ_α and γ_c, the coherent interface energy. We have confirmed that this behaviour is exhibited by all systems in which $m(c)$ increases monotonically. This led us to study system Ib in which $m(c) = 1+0.5c^2-2.5c^2(1-c)^2$ increases non-monotonically from $m(0) = 1$ to $m(1) = 1.5$, with a global minimum at $c\approx0.4$. Thus, in system Ib, the gradients in c and η_i are 'bunched up' at the incoherent boundary (see Fig. 1h), with a corresponding decrease in γ_i, which is about 1% lower than $(\gamma_\alpha + \gamma_c)$. The other boundaries in system Ib are essentially the same as those in system Ia, as confirmed by comparing Fig. 1(a,c,e) with Fig. 1(b,d,f), and by comparing their energies and widths in Table 2.

In order to see if GB width plays a role in our results, we studied system Ic, whose parameters were selected using the following logic: In diffuse interface theory involving a single variable [1,23], interfacial energy γ and width w are proportional to $(\kappa\Delta f)^{1/2}$ and $(\kappa\Delta f)^{1/2}$, respectively, where Δf is the height of the free energy barrier between the equilibrium phases; these relations hold also for our model with multiple order parameters, but only approximately; this is because Δf in our model scales only approximately with $\varepsilon m(c)$. Thus, we have studied system Ic, a variation of system Ia, in which the GB widths are half those in system Ia, without changing their energies appreciably. In this system, $m(c)$ is twice (and hence, Δf is about twice), and κ_η is half, as much as their respective values in system Ia.

For each boundary, its energy γ and width w are calculated from the profiles such as those in Fig. 1. In our model, since the energy of α and β phases within a grain is zero (see Eq. (2)), γ is numerically equal to F in Eq. (1) for an equilibrium system that contains only one planar interface of unit area. On the other hand, widths are defined operationally in each profile: for each field variable p ($p = c,\eta_1$ or η_2) we define a width $w_p = |x_2-x_1|$ where x_1 and x_2 are defined by $p(x_1) = 0.1$ and $p(x_2) = 0.9$. For the coherent boundary, we define w, the boundary width, by $w = w_c$, while for the others, we define it by $w = (w_{\eta_1} + w_{\eta_2})/2$.

A summary of the boundary energies and widths for these four different systems is given in Table 2: the value of $(\gamma_\beta-\gamma_\alpha)$ is nearly the same in systems Ia, Ib and Ic. Compared to system Ia, system Ib has a smaller value of γ_i, system Ic has smaller boundary widths for α-GB, β-GB and incoherent boundary, and system IIa has a smaller value of $(\gamma_\beta-\gamma_\alpha)$.

Table 2
Scaled energies (γ/N_V) and widths of boundaries in systems I(a–c) and IIa

System index	$m(c)$	κ_η	γ_α/N_V, w_α	γ_β/N_V, w_β	γ_i/N_V, w_i	γ_c/N_V, w_o
Ia	$1 + 0.5c^2$	1.0	0.732, 4.06	0.892, 3.33	1.066, 4.05	0.333, 4.45
Ib	$1 + 0.5c^2 - 2.5c^2(1-c)^2$	1.0	0.732, 4.06	0.891, 3.32	1.055, 4.00	0.33, 4.45
Ic	$2 + c^2$	0.5	0.732, 2.07	0.890, 1.75	1.066, 2.07	0.33, 4.45
IIa	$1 + 0.1c^2$	1.0	0.732, 4.06	0.768, 3.87	1.066, 4.06	0.33, 4.45

3.2. GB effects in a two-grain system

Fig. 2 shows the evolution of microstructure in an alloy of composition $c_o = 0.5$ in system Ia; in this simulation, two grains share two parallel planar boundaries (with periodic boundary conditions imposed along both dimensions). The initial composition fluctuations used in this simulation fall uniformly in the interval $\pm\,\delta_c$ with $\delta_c = 0.04$. For this system, γ_α, the α-GB energy is about 18% lower than γ_β (see Table 2). This difference provides the driving force, during early stages, for the GB to acquire species A; see the dark band at the GB in Fig. 2 for $t = 10$. This process of GB enrichment with species A also leads to the formation of a B-enriched layer (white band) followed by a faint A-rich band (dark grey) on either side of the boundary in this figure. During this time, the grain interior undergoes normal SD; the extent of this decomposition, however, is much smaller than that at the boundaries. For example, at $t = 10$, the highest and lowest compositions near the GB are about 0.63 and 0.32, respectively; their values in the grain interiors, however, are only about 0.54 and 0.46, respectively.

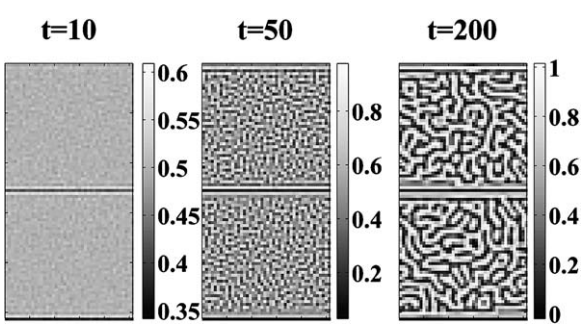

Fig. 2. Evolution of microstructure in a two-grain system (with periodic boundary conditions along both x and y axes) in system Ia for $t = 10$, 50 and 200, for an alloy of composition $c_o = 0.5$ and with initial fluctuations of $\delta_c = 0.04$. Note the different grey scales for these three microstructures.

At $t = 50$, the microstructure shows three bands at and near the GB in each grain (starting with the α band at the GB, followed by a β band and a second α band), coexisting with a grain interior exhibiting normal SD. Moreover, the decomposition is nearly complete everywhere. Further evolution results in coarsening of bands near GB's and spinodal microstructure in the grain interior. Such a coarsened microstructure is shown in Fig. 2 for $t = 200$.

3.3. Effect of ($\gamma_\beta - \gamma_\alpha$) and initial fluctuation

The microstructural evolution depicted in Fig. 2 may be described in terms of a competition between two different phenomena: (a) GB assisted phase separation and (b) normal SD in the grain interior. The former initiates a composition wave which travels into the grains, while the latter leads to the formation of a bicontinuous microstructure of A-rich and B-rich regions. Further, the former is faster than the latter. If normal SD were absent or when it takes place only to a small extent, the GB-initiated composition wave would continue to propagate into each grain, and the microstructure within each grain would consist entirely of alternating bands of α and β phases.

From the above description of SD in polycrystals, we may infer that the number of bands near the GB would be (a) higher if the normal SD in grain interiors can be delayed (e.g., by using smaller fluctuations (noise) in the initial configuration), and (b) lower if the driving force

($\gamma_\beta - \gamma_\alpha$) for the GB enrichment with species A is made smaller. Fig. 3, in which we compare the microstructures at $t = 50$ in three different systems, illustrates that both these inferences are true. System Ia with $m(c) = 1+0.5c^2$ (Fig. 3a) represents high driving force for the GB enrichment, and high initial noise of $\delta_c = 0.04$. It shows three bands in each grain: an α-GB band, followed by a β and a second α band. The system depicted in Fig. 3b has the same driving force (it is still system Ia), but evolved from an initial configuration which had a lower initial fluctuation of $\delta_c = 0.01$; normal SD in the grain interior is therefore delayed, providing an opportunity for the GB assisted composition wave to penetrate further into the grains and leading to five bands (the fifth band of α phase is barely continuous, but can still be discerned) in each grain near the GB. Now, with the same lower initial noise of $\delta_c = 0.01$, if the driving force for the initial GB-enrichment with species A is reduced (in system IIa, for which $m(c) = 1+0.1c^2$), we find only four bands in Fig. 3c.

The microstructures such as those presented in Fig. 3 may be analysed quantitatively by plotting the difference $(c_p - c_o)$ as a function of distance from the GB, where c_p is the average composition within a layer parallel to the GB and c_o is the alloy composition. Such a plot for system Ia is shown in Fig. 4 for three different times. This figure shows that the composition wave is initiated at the GB, and propagates into the grain interiors; further, for a given time, this composition wave also decays with distance from the GB.

We have monitored $R_1(t)$, the first zero of the $(c_p - c_o)$ profile, and plotted it in Fig. 5 as a function

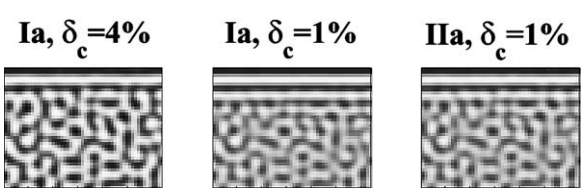

Fig. 3. Microstructures at $t = 100$ from three different simulations, showing the effect on the number of GB bands of ($\gamma_\beta - \gamma_\alpha$) and initial noise. Systems in the left and middle figures differ in the initial fluctuations, while those in the middle and right figures differ in ($\gamma_\beta - \gamma_\alpha$). For clarity, we show only 128 × 96 grids near a grain boundary, which is at the top.

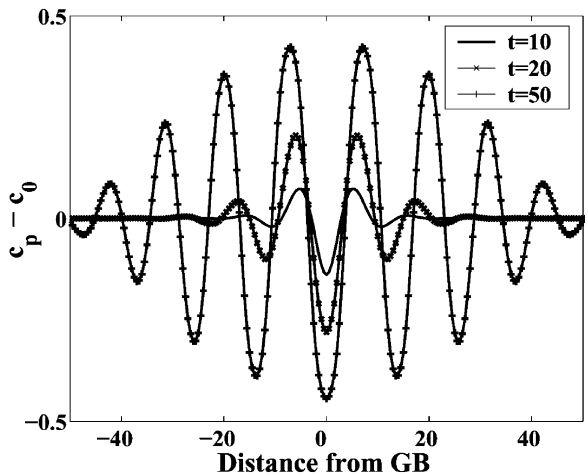

Fig. 4. The difference $(c_p - c_o)$ between the average composition c_p of each layer parallel to the GB and alloy composition c_o as a function of distance from the GB for different times. The plots are for system Ia with $\delta_c = 0.04$.

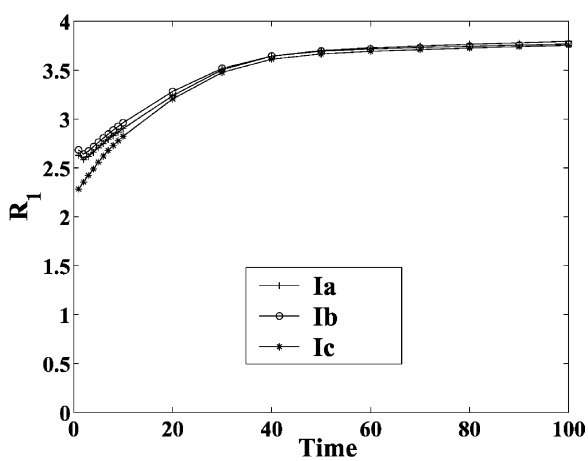

Fig. 5. The dependence of R_1, the first zero in the plots of $(c_p - c_o)$ (see the previous figure), on time for the three different systems: Ia, Ib and Ic.

of time for systems Ia, lb and Ic. It is clear that R_1 increases with time, before stabilizing towards late stages. More importantly, the $R_1(t)$ behaviour is essentially the same in these three systems, indicating that differences in GB widths (in system Ic) or in incoherent boundary energy (in system Ib) do not play a significant role in determining the formation of GB-bands.

3.4. Number of GB bands

A different analysis of the GB-initiated composition wave can be used for estimating the number of GB bands in the microstructure. This analysis is based on the extent of decomposition defined by:

$$f_D = \frac{\int_{V_b}(c-c_o)^2 dV}{V_b[f_\alpha(c_\alpha-c_o)^2 + f_\beta(c_\beta-c_o)^2]} = \frac{\int_{V_b}(c-c_o)^2 dV}{V_b c_o(1-c_o)}$$

where V_b is the volume of interest, $f_\alpha = 1-c_o$ and $f_\beta = c_o$ are the equilibrium volume fractions of α and β phases, respectively; we have used $c_\alpha = 0$ and $c_\beta = 1$ in this equation. By definition, $f_D = 0$ for a homogeneous alloy, and $f_D = 1$ at equilibrium.

The hypothesis we wish to test is that the GB initiated composition wave (and the associated band formation) progresses into the grain until it encounters a region that has decomposed to a significant extent. For this purpose, f_D is estimated separately for each of the bands in a simulation of GB-assisted SD, which is carried out with no initial composition fluctuation within the grains, so that the composition waves would continue to propagate into them. In Fig. 6, these f_D values for individual bands are plotted as a function of time, and compared with similar plots for two bulk simulations (with no GB) of system Ia starting with an initial noise of $\delta_c = 0.04$ and $\delta_c = 0.01$.

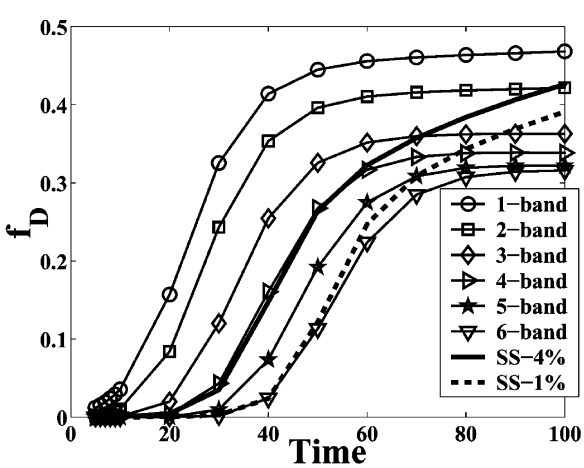

Fig. 6. The extent of decomposition f_D as a function of time; plots are shown for bands 1 through 6 from a simulation of system Ia with a GB, and for two bulk (single crystal, referred to as 'SS' in the legend) simulations with initial fluctuations of $\delta_c = 0.04$ (thick continuous line) and $\delta_c = 0.01$ (thick dashed line).

In Fig. 6, the f_D curves for the first three bands are to the left of those for the bulk systems, indicating that decomposition has progressed much faster in these bands. More importantly, the curve for the fourth band lies close to that for the bulk simulation with a higher initial noise $\delta_c = 0.04$. From our hypothesis, this result implies that a fourth band is unlikely to form in this system; Fig. 5a, for system Ia with $\delta_c = 0.04$, indeed shows only three bands. In a similar way, since f_D curve for the sixth band is close to that for the bulk system with $\delta_c = 0.01$, we may expect only five bands for this system; again, Fig. 3b shows that this is indeed the case.

3.5. Polycrystalline alloys

A prior simulation is used to produce the polycrystalline structure used in this part of the study. In this simulation, many (typically 50) circular grains whose scaled radii are randomly chosen between 15 and 20, are placed in the simulation box. This simulation used $c_o = 0$ (α phase) and $m(c) = 1$ and produced a polycrystal. Simulations of SD started with this microstructure, with a uniform initial composition of $c_o = 0.5$ and with an initial flucutation of $\delta_c = 0.04$. The results are presented for system Ia; the results for the other systems are similar.

The microstructural evolution in polycrystals is as shown in Fig. 7, and is similar to that shown in Fig. 2 for the two-grain case. By $t = 10$, the GB's are enriched with species A, thus converting them into α-GB's; on either side of this GB band, a β band is already visible. The accompanying grey-scale shows that the GB-initiated SD has progressed to a considerable extent, while the normal SD in the grain interiors is barely visible. For example, we find for $t = 10$, composition in regions near GB have $c_o \pm 0.15$, while those in the interior are $c_o \pm 0.04$. At $t = 50$, the microstructure shows that GB-initiated SD has progressed to yield compositions as low as 0.02 at the GB and as high as 0.98 in the adjacent β bands. In the interior, though, the comparable figures are 0.05 and 0.95,

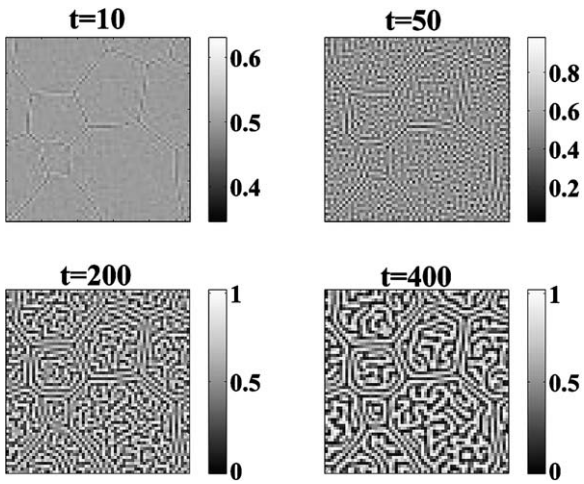

Fig. 7. Microstructural evolution in a polycrystalline alloy of composition $c_o = 0.5$ in system Ia ($m(c) = 1+0.5c^2$) with $\delta_c = 0.04$. The times are indicated above the microstructures. Note the different grey scales in these figures.

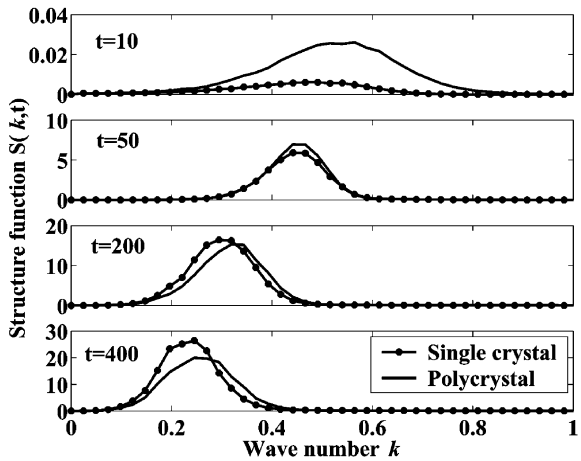

Fig. 8. Circularly averaged structure factor $S(k)$ as a function of wave number k for a single and a polycrystal at different times. The plots are for system Ia with $\delta_c = 0.04$ (same system as in the previous figure).

indicating that progress of SD is only slightly behind that at GB's.

In the late stage microstructure at $t = 200$, the two phases have reached their equilibrium compositions of $c = 0$ and $c = 1$. The α and β bands formed during the early stages are still visible, and coexist with the normal SD in the grain interiors. The microstructure at $t = 400$ is coarser than that at $t = 200$. Interestingly, this microstructure also shows the α-GB with only one band of β on either side, implying that the third and innermost α band had disintegrated. Finally, since the original GB's become α-GB's very early, their migration is not preferred since it would take them through the β band, in which their energy is higher. Thus, grain growth is effectively arrested during the decomposition process.

In Fig. 8, we have plotted the spherically averaged structure factor $S(k)$ as a function of wave number k at different times, for both single and polycrystals. At $t = 10$, $S(k)$ for the polycrystal is well above that for the single crystal, indicating the much larger extent of decomposition in the former. As we have seen above, this is clearly a result of the GB assisted phase separation being much faster than normal SD in the single crystal (and in the grain interiors). Further, the wave vector k_m for which $S(k)$ exhibits a peak is larger for the polycrystal ($k_m = 0.56$) than in the single crystal ($k_m = 0.46$). This implies that the length scale of GB-assisted phase separation is smaller than that of normal SD. At $t = 50$, $S(k)$ for the polycrystal is just barely above that for the single crystal, and k_m values are nearly the same at $k_m \approx 0.44$.

At $t = 200$ and $t = 400$, $S(k)$ curves for the single crystal are to the left of (and narrower and more peaked than) those for the polycrystal. This result implies a slower coarsening of GB bands, since $S(k)$ is averaged over the entire microstructure, and since the microstructure in the grain interiors is essentially the same as that due to normal SD in single crystals (and hence must have coarsened at the same rate). Slower coarsening of GB bands can be explained by the smaller difference in interface curvature across adjacent bands.

4. Discussion

4.1. Microstructural evolution

Our most important result is that, for systems with constant atomic mobility, the GB effects during SD are in the form of bands of α and β phases near the GB's. As a result, all the original GB's become, in the final microstructure, either α GB's

or incoherent α–β boundaries, depending on whether $(\gamma_\alpha + \gamma_c)$ is less than or equal to γ_i (such as in systems Ia, Ic and IIa) or otherwise (e.g. system Ib). Further, due to the presence of α and β bands, migration of an α GB normal to itself would take it through the β band, in which its energy is higher. Therefore, migration of GB's (and hence, grain growth) is effectively prevented by the GB bands.

The acquisition of species A at the GB gives the appearance of the GB being 'wetted' by the α phase. However, energies of various interfaces in Table 2 show that equilibrium wetting of GB by the α phase is impossible: wetting requires either $\gamma_\beta > (\gamma_i + \gamma_c)$ or $\gamma_\beta > (\gamma_i + 2\gamma_c)$, depending on whether $\gamma_i < (\gamma_\alpha + \gamma_c)$, or otherwise. Neither condition holds in any of the systems in Table 2. Thus, the wetted appearance of the GB in Fig. 2 can only be attributed to kinetic reasons: the atomic mobility M is a constant in our simulations. Indeed, in our preliminary work on systems with higher M at the GB than in the interiors, phase separation at the GB precedes that in the interior, resulting in alternating 'beads' of α and β phases *along* the GB.

4.2. Assumptions in the model and their implications

We have assumed, for this study, a constant atomic mobility M; i.e., it is the same at the GB's as well as in the grain interiors. This assumption, used primarily due to computational ease, is rather restrictive, since it neglects the enhanced (by several orders of magnitude [25]) atomic mobility at high angle grain boundaries in metallic systems. However, examples of GB's with similar atomic mobilities as in the bulk may be found in twin boundaries, stacking faults and small angle boundaries in metallic alloys. Thus, our results in Section 2, particularly for planar boundaries between grains, are applicable to these special cases. However, our search for reports of experimental studies of SD at and near such special boundaries has not been successful.

The use of position-dependent mobility, while computationally burdensome, is not forbiddingly so. Zhu et al. [24], in their study of SD in bulk systems with variable M, used a novel variant of the semi-implicit Fourier technique. Our own ongoing research uses their method for studying systems with enhanced atomic mobility at the GB. Thus, our results presented in this paper may be thought of as a first approximation of GB effects on SD, and as a benchmark for comparing those from simulations of systems with GB-enhanced mobility.

Another assumption in the model is that all the interfacial energies (γ_c, γ_i, γ_α, γ_β) are isotropic. Thus, the model is incapable of studying systems in which one has different kinds of, for example, grain boundaries with different energies. However, we may point out that there exist phase field formulations for studying systems anisotropic interfacial energies [26,27], and polycrystals with anisotropic GB energies [28,29], which may be fruitfully combined in a future study.

While our simulations studied 2D systems, our main result that bands are formed when atomic mobility is independent of position is also applicable to 3D systems. Thus, the bands, which extend along the GB, are one-dimensional in our 2D simulations, while they would be two-dimensional in 3D systems. The grain interior, which exhibits normal SD microstructure, would continue to show the same behaviour in 3D systems as well.

4.3. Comparison with other studies

Some of our results on GB effects are similar to those observed in studies [7–14] of the effect of a free surface on SD. This is because the underlying physics is the same; just as a positive difference in GB energies $(\gamma_\beta - \gamma_\alpha)$ provides the driving force for enrichment of species A at the GB, a positive difference in surface energies $(\gamma_\beta^s - \gamma_\alpha^s)$, leads to enrichment of species A at the surface, and sets off a composition wave which travels into the bulk. Further, when atomic mobility is constant (i.e., it is *not* enhanced at the surface), the final microstructure exhibits alternating bands near the surface, even in systems in which the surface can only be partially wetted by species A at equilibrium [10,11]. Similar to our results in Section 3, the number of surface bands also increases when the initial composition fluctuation is smaller [8]. Since the GB's in our system remain stationary (just like

a free surface), these similarities between GB and surface effects are not surprising. However, the lack of GB movement in the present study is due mainly to the pinning effect of the GB bands, and not due to their inherent inability to migrate. Indeed, our work [30] on systems with GB-enhanced atomic mobility shows that a GB may migrate under suitable conditions, and form a discontinuous transformation front separating the undecomposed grain (ahead of it) from the decomposed region, where the two product phases are in the form of alternating lamellae; such discontinuous microstructures have also been observed in experimental SD systems such as Au–Ni [31,32] and Cu–Ni–Fe [33].

Recently Hu and Chen [17] have used a phase field model which integrates defect and phase microstructures, and showed that even in an alloy outside the spinodal, the interaction between the solute and dislocation may give rise to spontaneous nucleation (without the aid of thermally induced composition fluctuation) of coherent precipitates. Though their model can be used for studying dislocation effects on SD, their studies have so far been on precipitation in alloys outside the spinodal.

Moore et al. [18] studied the effect of a precipitate plate on SD, and have reported alternating bands (similar to those observed near GB's in our study) in an Al-22 atomic% Ag alloy. On solutionizing this alloy at 560 °C and aging at 350 °C, it undergoes, in addition to SD, a precipitation process that produces plates of the equilibrium γ phase (with a composition of nearly 60 atomic% Ag). As a result of this precipitation process, an Ag-poor region develops on either side of the γ plates. This Ag-poor region further leads to an Ag-rich band, an Ag-poor band, and a third faint Ag-rich band in the inter-plate regions undergoing SD. Despite their location near a precipitate, the origin of these bands is the same as in our study: while the bands are caused by Ag-depletion near the plates in the Al–Ag alloy, they are caused by enrichment of species *A* (and a consequent depletion of *B*) at the GB in our study.

5. Conclusions

1. We have developed a phase field model of a polycrystalline binary alloy by combining the Cahn–Hilliard model [1] for a compositionally inhomogeneous alloy with a model of polycrystals due to Fan and Chen [2].
2. We have used this model for studying GB effects on SD in systems in which the atomic mobility at GB is the same as that in the grain interior.
3. In systems in which the GB-energy of the α phase is lower than that of the β phase, the primary effect of a GB is the formation of alternating bands of the product phases parallel to the boundary. At the end of the decomposition, the microstructure exhibits these GB-bands coexisting with a normal SD microstructure in the grain interior.
4. The number of bands has been rationalized in terms of the driving force for band formation ($\gamma_\beta - \gamma_\alpha$), and the strength of initial composition fluctuations. Formation of bands also effectively arrests grain growth.

Acknowledgements

We thank the Council of Scientific and Industrial Research, Government of India, for financial support for this work. We gratefully acknowledge fruitful discussions with Professors V. Jayaram, P.W. Voorhees, P. Bellon and F. Haider.

References

[1] Cahn JW, Hilliard HE. J. Chem. Phys. 1958;28:258.
[2] Fan D, Chen L-Q. Acta Mater. 1997;45:3297.
[3] Binder K. In: Kostorz G, editor. Phase transformations in materials. Transformation in materials. Weinheim: Wiley-VCH; 2001.
[4] Binder K. In: Haasen P, editor. Materials science and technology. Transformation in materials, 5. Weinheim: VCH; 1991.
[5] Fratzl P, Penrose O, Lebowitz JL. J. Stat. Phys. 1999;95:1429.
[6] Bray AJ. Adv. Phys. 1994;43:357.
[7] Ball RC, Essery RLH. J. Phys.: Cond. Matter 1990;2:10303.

[8] Marko JF. Phys. Rev. E 1993;48:2681.
[9] Bastea S, Pun S, Lebowitz JL. Phys. Rev. E 2001;63:041513.
[10] Frisch HL, Nielaba P, Binder K. Phys. Rev. E 1995;52:848.
[11] Puri S, Binder K. Phys. Rev. Lett. 2001;86:1797.
[12] Puri S, Binder K, Frisch HL. Phys. Rev. E 1997;56:6991.
[13] Puri S, Binder K. J. Stat. Phys. 1994;77:145.
[14] Fischer HP, Maass P, Dieterich W. Phys. Rev. Lett. 1997;79:893.
[15] Geng C, Chen L-Q. Surf. Sci. 1996;355:229.
[16] Geoghegan M, Ermer H, Jungst G, Krausch G, Brenn R. Phys. Rev. E 2000;62:940.
[17] Hu SY, Chen L-Q. Acta Mater. 2001;49:463.
[18] Moore KT, Johnson WC, Howe JM, Aaronson HI, Veblen DR. Acta Mater. 2002;50:943.
[19] Reedhill RE, Abbaschian R. Physical metallurgy principles. Boston: PWS-Kent, 1991.
[20] Cahn JW. Acta Metall. 1961;9:795.
[21] Tikare V, Holm EA, Fan D, Chen L-Q. Acta Mater. 1999;47:363.
[22] Phillips R. Crystals, defects and microstructures. Cambridge: Cambridge University Press, 2001.
[23] Allen SM, Cahn JW. Acta Metall. 1979;27:1085.
[24] Zhu J, Chen L-Q, Shen J, Tikare V. Phys. Rev. E 1999;60:3564.
[25] Shewmon PG. Diffusion in solids. Pennsylvania: TMS, 1989.
[26] Kobayashi R. Physica D 1993;63:410.
[27] Abinandanan TA, Haider F. Phil. Mag. A 2001;81:2457.
[28] Kazaryan A, Shen C, Wang Y, Patton BR. In: Turchi PEA, Gonis A, editors. Phase transformations and evolution in materials. Pennsylvania: TMS; 2000. p. 89.
[29] Kobayashi R, Warren JA, Carter WC. Physica D 2000;140:141.
[30] Ramanarayan H, Abinandanan TA. 2003 [Submitted to Acta Mater].
[31] Gust W, Predel B, Nguyen-Tat T. Z Metall. 1976;67:110.
[32] Zhao J, Notis M. Met. Trans. A 1999;30A:707.
[33] Gronsky R, Thomas G. Acta Metall. 1975;23:1163.